Supplementary Information

PLGA protein nanocarriers with tailor-made fluorescence/MRI/PET imaging modalities

Yajie Zhang,[a] Miguel García-Gabilondo,[b] Alba Grayston,[b] Irene V. J. Feiner,[c] Irene Anton-Sales,[a] Rodrigo A. Loiola,[d] Jordi Llop,[c,e] Pedro Ramos-Cabrer,[f,g] Ignasi Barba,[h] David Garcia-Dorado,[h#] Fabien Gosselet,[d] Anna Rosell*[b] and Anna Roig*[a]

a. *Institut de Ciència de Materials de Barcelona (ICMAB-CSIC), 08193 Bellaterra, Catalonia, Spain. E-mail: anna.roig@csic.es*
b. *Neurovascular Research Laboratory, Vall d'Hebron Institut de Recerca, Universitat Autònoma de Barcelona, 08035 Barcelona, Catalonia, Spain. E-mail: anna.rosell@vhir.org*
c. *Radiochemistry and Nuclear Imaging Group, CIC biomaGUNE, Basque Research and Technology Alliance (BRTA), 20014 San Sebastian, Guipúzcoa, Spain.*
d. *University of Artois, Blood-Brain Barrier Laboratory (BBB Lab), UR2465, F-62300 Lens, France.*
e. *CIBERES, Centro de Investigación Biomédica en Red, 28029 Madrid, Spain.*
f. *Magnetic Resonance Imaging Laboratory, CIC biomaGUNE, Basque Research and Technology Alliance (BRTA), 20014 San Sebastian, Guipúzcoa, Spain.*
g. *Ikerbasque, Basque Foundation for Science, 48013 Bilbao, Spain.*
h. *Cardiovascular Diseases Research Group, Vall d'Hebron University Hospital and Research Institute, Universitat Autònoma de Barcelona, 08035 Barcelona, Spain.*

 # In memoriam of our colleague Dr. Garcia-Dorado who passed away on August 16th 2019.

Figure S1. ATR-FTIR spectra of commercial PLGA and modified PLGA-NH_2/PLGA-DFO products confirmed their similar chemical structure and the successful modification. a) commercial PLGA, as synthesized PLGA-NH_2 and PLGA-DFO, inset is the magnified spectra of the 3500 -3000 cm^{-1} range; b) commercial p-NCS-Bz-DFO.

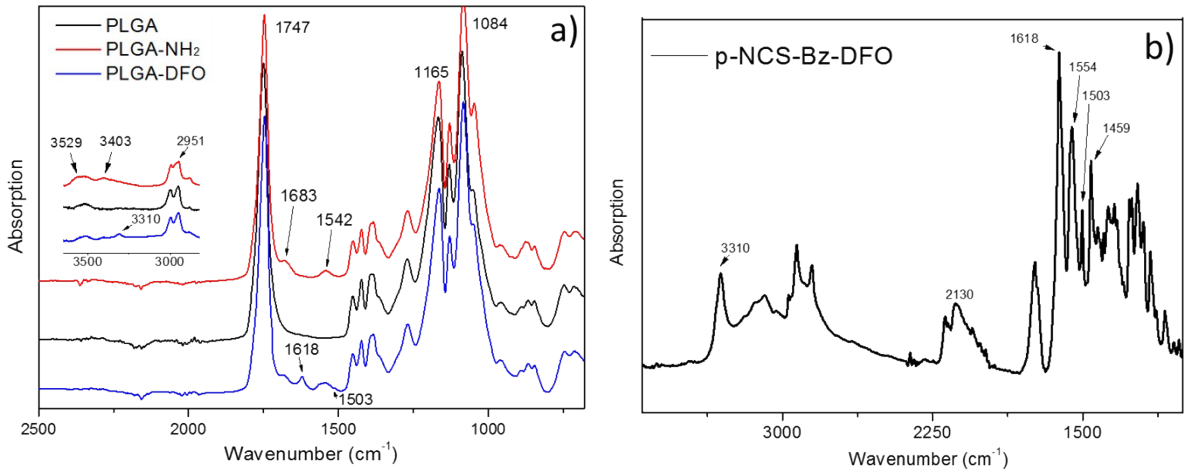

Both of PLGA and PLGA-NH_2 showed the typical bands at 1084 cm^{-1}, 1165cm^{-1} and 1747 cm^{-1} attributed to the C=O stretch and C-O asymmetrical and symmetrical stretches of the ester chain of the PLGA, and the C-H stretch bands of the alkane near 2951 cm^{-1}. The bands and shapes similarities of the three spectra implied that the main molecular chain of PLGA was not affected by the modifications. Some new peaks appear in the spectrum of PLGA-NH_2, a band at 1542 cm^{-1} associated with the NH bending of the secondary amide II, at 1683 cm^{-1} associated to the C=O stretching of the secondary amide I, at 3529 cm^{-1} and 3403 cm^{-1} shown in the inset attributed to the asymmetrical and symmetrical stretches of -NH_2. These correlation absorption bands successfully demonstrated the formation of a secondary amide at the -COOH terminal of PLGA with one -NH_2 group of ethylenediamine, meanwhile the -NH_2 group on the other side of ethylenediamine served as the terminal function group of PLGA chain.

When compared to the ATR-FTIR spectrum of PLGA-NH_2, new bands appeared in the spectrum of PLGA-DFO. Bands at 1618 cm^{-1}, 1554 cm^{-1} and 1503 cm^{-1} attributed to the C=C stretches of the backbone of aromatic ring, the band at 3310 cm^{-1} corresponds to the NH stretching of the secondary amide, all these structure information are consistent with those in commercial p-NCS-Bz-DFO, indicating the successful conjugation of DFO. The disappearance of N=C=S stretching band at 2130 cm^{-1} in the PLGA-DFO spectrum also demonstrated the reaction of –NCS with –NH_2.

Figure S2. a) Calibration curve of absorbance at 390nm of different concentrations of ethylenediamine (-NH2) with an excess amount of fluorescamine; b) UV-Vis absorption of 0.083 mM of PLGA-NH_2 product with an excess amount of fluorescamine; c) UV-Vis absorption of 0.25 mM of PLGA-DFO product with/without fluorescamine.

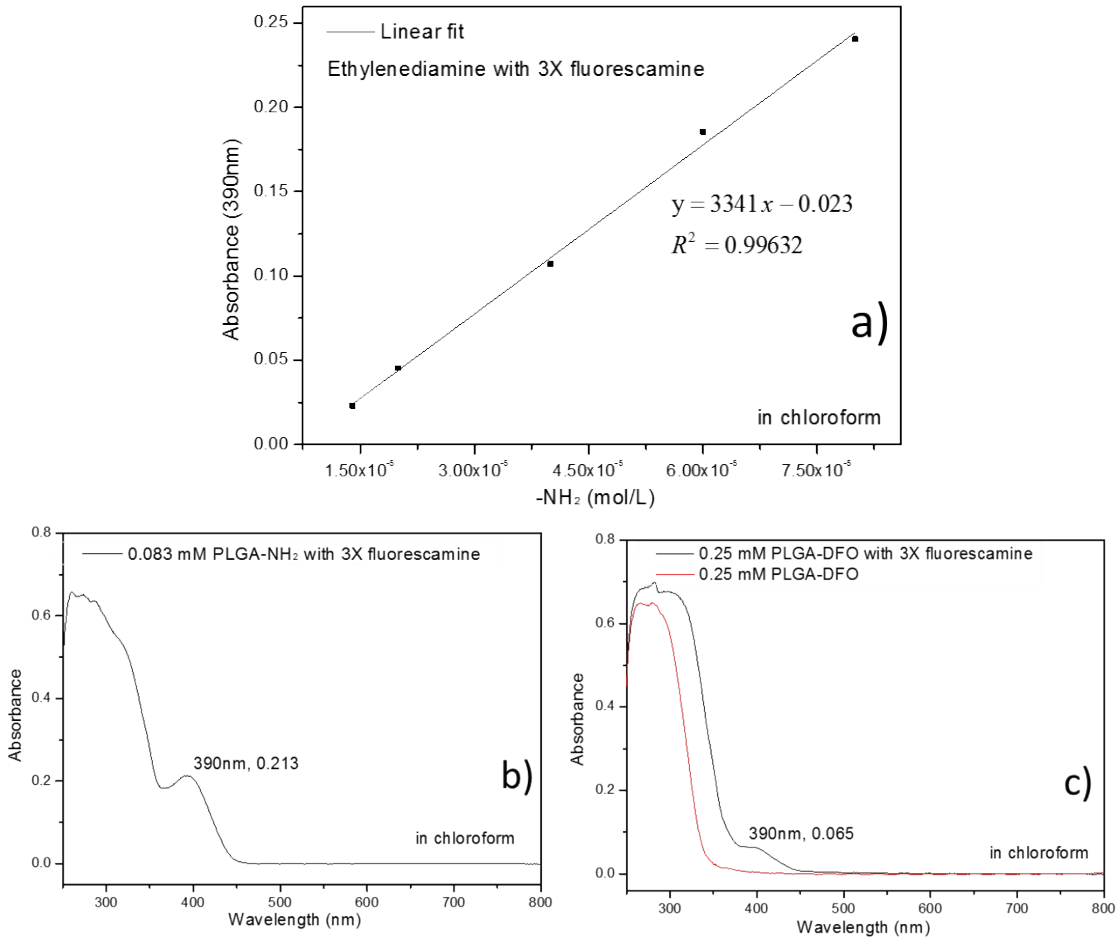

Figure S3. a) Fluorescence intensity-absorbance curves of PLGA-Fluram and reference Coumarin 153 for quantum yield measurements; b) photostability evaluation of NC.PLGA-Fluram (NC-4) under confocal microscope at 10% laser power, fluorescence intensity expressed as the percentage vs. time 0.

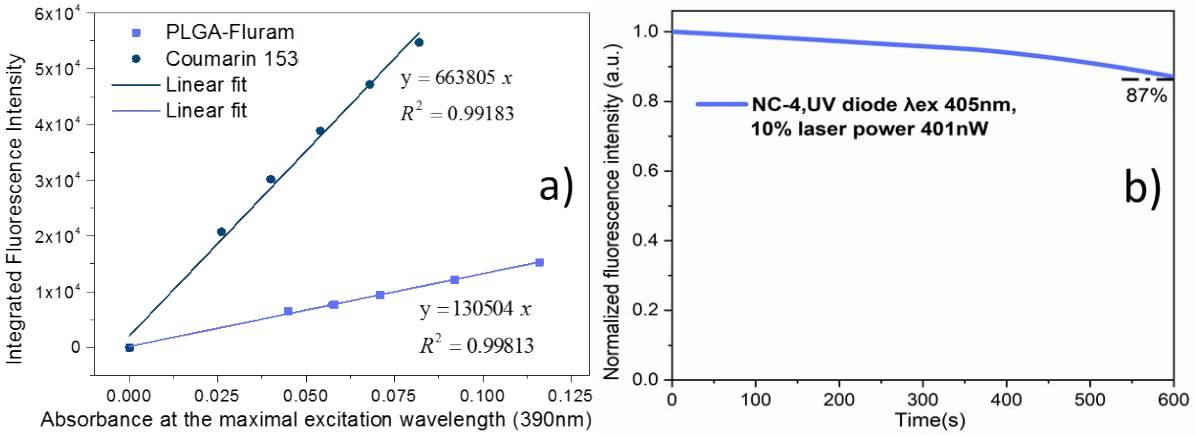

The quantum yield of the PLGA-Fluram was measured by the Williams' method. Briefly, a series of PLGA-Fluram solutions in chloroform were prepared with gradient concentrations. An excitation wavelength of 390 nm was determined to generate the highest emission intensity. The fluorescence spectra were collected for the series of solutions in the 10 mm fluorescence cuvette. The integrated fluorescence intensity, which is the area of the fluorescence spectrum, was calculated. Then UV-vis absorbance spectra were collected with the same solutions and the absorbance at the maximal excitation wavelength within the range of 0.01–0.1 Abs units was noted. The graphs of integrated fluorescence intensity vs. absorbance were plotted. The quantum yield of the PLGA-Fluram was calculated according to the equation $\Phi s = \Phi_r(\frac{Slopes}{Slope_r})(\frac{ns}{n_r})^2$ where, Φ = quantum yield; slope = slope of the linear fit obtained from the plot of intensity versus absorbance; n = refractive index of the solvent; s = subscript to denote the sample, and r = subscript to denote the reference. Coumarin 153 (quantum yield = 90% in cyclohexane) was used as the reference.

Figure S4. a) UV-Vis absorption spectra of PLGA/Cy7.5 samples; b) Quantification of fluorescence intensity of PLGA-Cy7.5 and free Cy7.5 in DMSO by IVIS at the λex/λem of 710/820 nm.

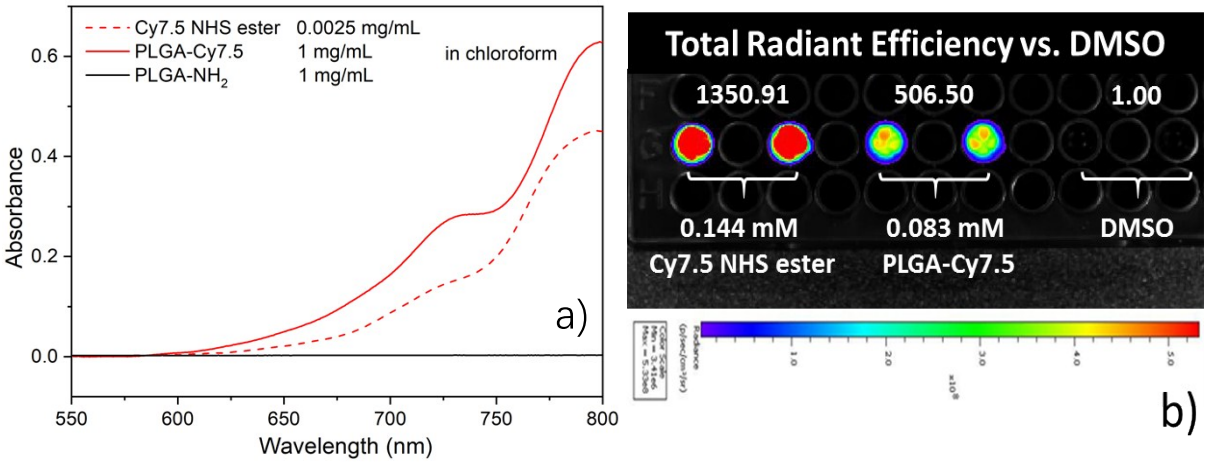

Figure S5. TEM images of the SPIONs with different diameters (6 nm and 9 nm). The size distribution histogram was assembled by measuring the diameter of the ~300 nanoparticles from several TEM images using ImageJ.

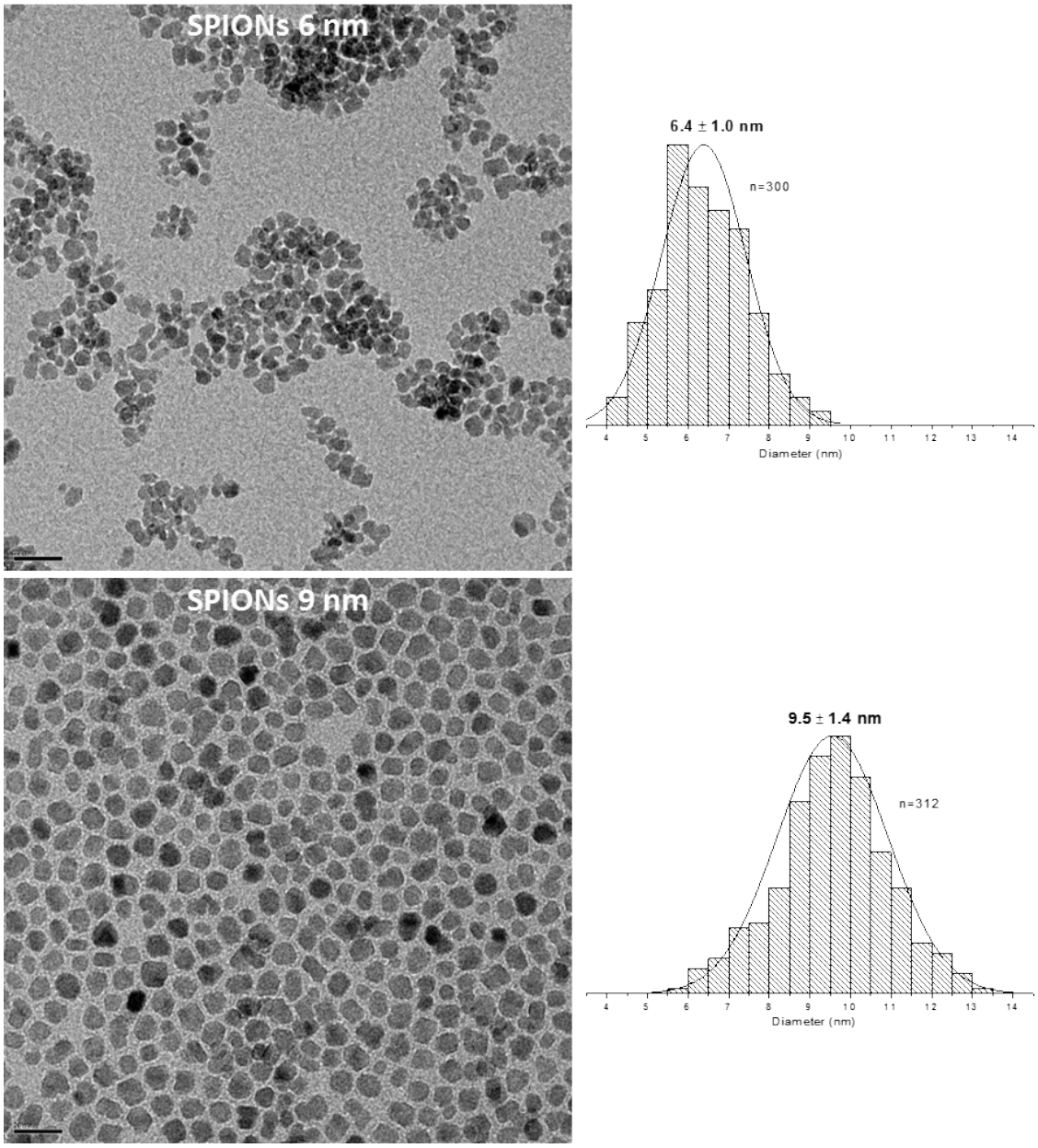

Figure S6. a) TGA curves of oleic acid coated SPIONs and non-coated SPIONs samples; panels a1) and a2) b) SQUID measurements of OA-SPIONs samples, the mass magnetization was expressed as emu/g pure SPIONs.

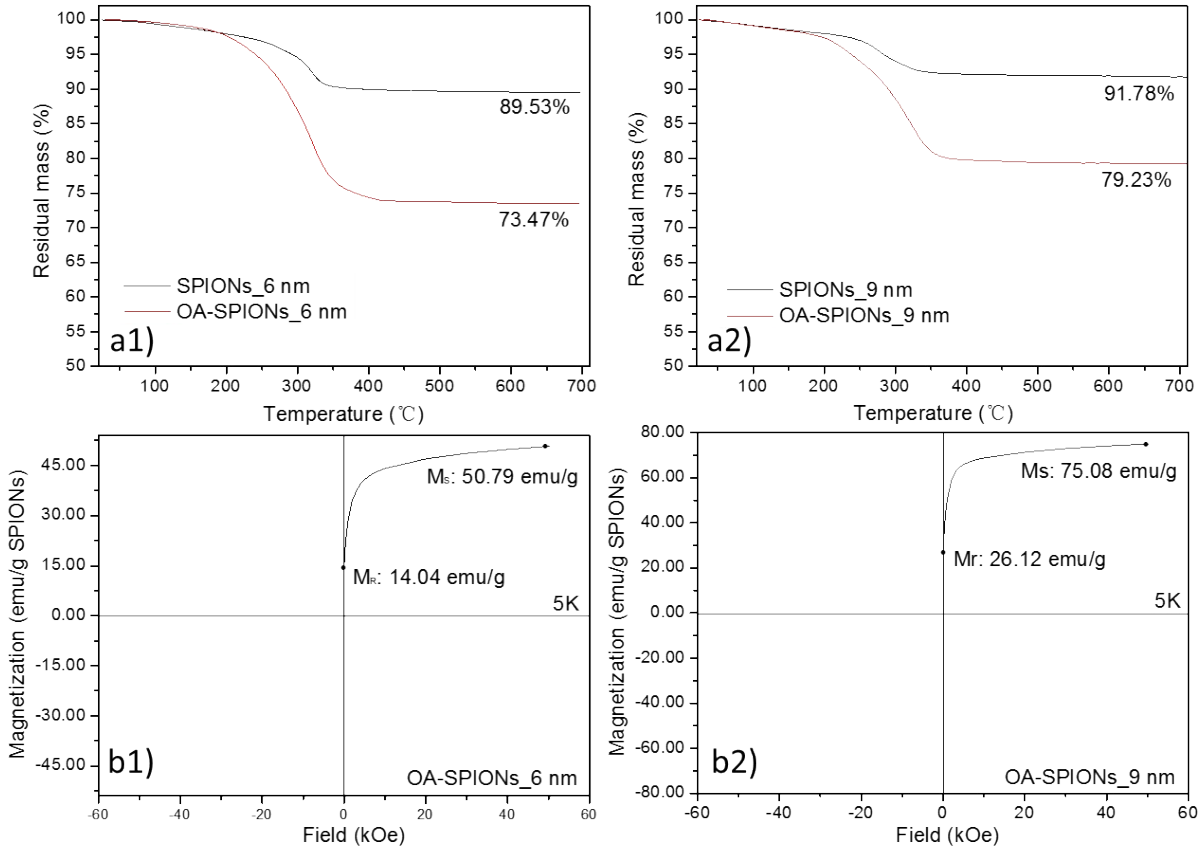

It is reasonable to consider that in air atmosphere at 700 °C the difference of residual mass between SPIONs and OA-SPIONs was attributed to the degradation and evaporation of the oleic acid molecules. In other words, the residues at 700 °C in air are the same substance for OA-SPIONs and SPIONs. So we proposed a method to calculate the SPIONs mass fraction of the OA-SPIONs samples. Here we designated the SPIONs mass fraction of OA-SPIONs samples as x, mass of OA-SPIONs as a g and residual mass fraction of SPIONs and OA-SPIONs samples at 700 °C as b and c, respectively. So there is: $a \cdot x \cdot b = a \cdot c$, $x = c/b$ (b and c are given by TGA data). Then: SPIONs_6 nm in OA-SPIONs: 82.06%, SPIONs_9 nm in OA-SPIONs: 86.33%.

Figure S7. SEM images of lyophilized the several types of PLGA nanocapsules that listed in Table 1.

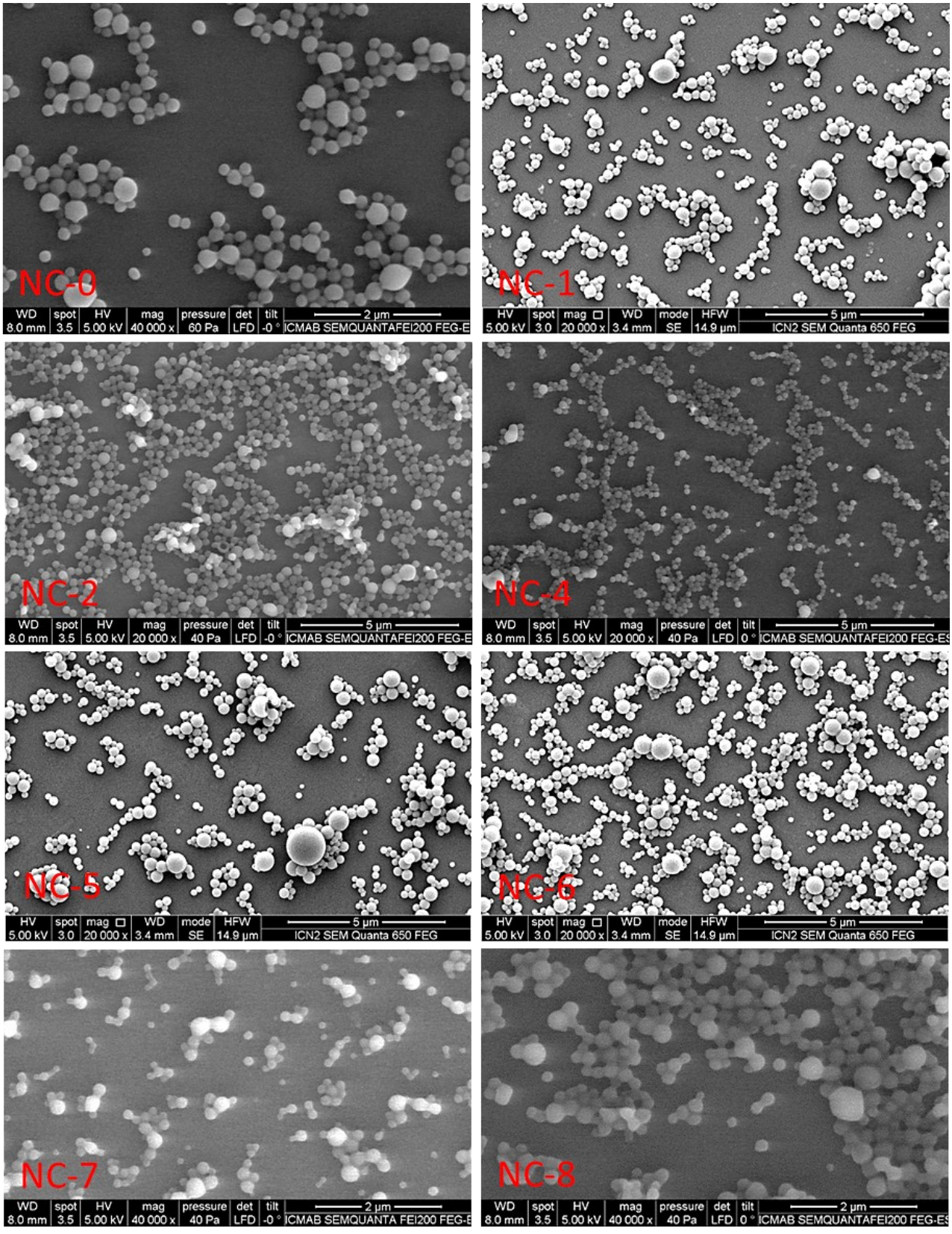

Figure S8. Quantitative region of interest analysis of the dynamic activity change in bladder. Time-activity curves of bladder upon i.v. injection of NC.89Zr-DFO-PLGA over 3 hours. (n = 2)